https://doi.org/10.5194/nhess-2024-131
Preprint. Discussion started: 18 September 2024

Natural Hazards and Earth System Sciences
Discussions

Coupled GPU-based Modeling of Dynamic-Wave Flow and Solute Transport in Floods with Cellular Automata Framework

Hsiang-Lin Yu[1,2], Tsang-Jung Chang[1,2,3]

[1]Dept. of Bioenvironmental Systems Engineering, National Taiwan University, Taipei, 106, Taiwan
[2]Hydrotech Research Institute, National Taiwan University, Taipei, 106, Taiwan
[3]Center for Weather and Climate Disaster Research, National Taiwan University, Taipei, 106, Taiwan

Correspondence to: Tsang-Jung Chang (tjchang@ntu.edu.tw)

Abstract. To achieve efficient modeling of flood flow and subsequent solute transport in real-world flood events, the present study couples the CA-based shallow water flow (SWFCA) solver of Chang et al. (2022) with a CA-based advanced solute transport (ASTCA) solver as a novel coupled approach. This coupled approach is GPU-parallelized by using OpenCL 2.1 under Nvidia CUDA to enhance efficiency. The accuracy of the coupled approach is verified and compared with a popular finite-volume-based coupled approach consisting of a Godunov-type FV-HLLC model for flood flow and a Godunov-type FV-TVD model for solute transport through four test cases. The efficiency of the coupled approach is next assessed through three real-world flood cases with massive computational cells. From the simulated results, the ASTCA solver is found to have better accuracy than the state-of-the-art FV-TVD model. Regarding the efficiency, the SWFCA and ASTCA solvers respectively outperform the FV-HLLC and FV-TVD models by 1.28-1.33 and 2.90-3.33 times. After GPU parallelization, the SWFCA solver, ASTCA solver, and CA-based coupled approach respectively speed up the simulations by 57.64-76.23, 53.55-69.88, and 56.32-74.15 times, which is a remarkable progress as the simulations are performed on a PC with a normal graphic card. Hence, the proposed approach is a useful tool for real-world flood flow and solute transport simulations.

1 Introduction

Flood inundation is one of the major natural disasters worldwide, which not only threatens lives and inundates properties, but also drifts wastes with fast-moving water flows and subsequently impacts people's health (Addison-Atkinson et al., 2022). Over the last decade, the rapid development of high-performance computing resources and the convenient availability of high-quality topographic/hydrologic datasets have led to more and more applications to conduct shallow water flows and solute transport in complicated real-world flood inundation problems. Such complicated real-world problems always require high-resolution meshes in large spatial domains, sometimes having a large number of simulations from probabilistic viewpoints. As a consequence, the demands of using accurate and effective models to simulate real-world shallow water flows and subsequent solute transport are dramatically increasing as many serious flooding events have occurred all over the world.

https://doi.org/10.5194/nhess-2024-131
Preprint. Discussion started: 18 September 2024


Natural Hazards and Earth System Sciences Discussions

Generally speaking, such demands can be fulfilled by coupling a shallow water flow model and a passive solute transport model (Addison-Atkinson et al., 2022). In terms of the shallow water flow models, they either solve the full or simplified versions of the two-dimensional (2D) shallow water equations (SWEs) (Castro-Orgaz and Hager, 2019). In the past two decades, various numerical methods have correspondingly been proposed to numerically solve the 2D SWEs, which can be categorized into mesh-based and meshless models. For the mesh-based models, finite difference methods, finite element methods, and finite volume (FV) methods are the three popularly used models, as extensively summarized by Toro et al. (2001) and Castro-Orgaz and Hager (2019). In terms of the meshless methods like smoothed particle hydrodynamics (SPH) models (Chang et al., 2011; Kao and Chang, 2012), Chang et al. (2014; 2016; 2024) and Sarkhosh and Jin (2021) have an extensive summary on them. Among these models, FV methods are one of the most popular modeling methods because of their strong capabilities in handling complex flow transitions such as hydraulic jumps/drops and wet-dry interfaces (Yu and Chang, 2021; Zhao and Liang, 2022). Although these FV methods can simulate complex conditions with transcritical flows and wet-dry interfaces with good accuracy (Martins et al., 2018), these FV methods are still time-consuming especially for real-world applications, especially for FV models with an implicit time integration (Chang et al., 2022).

As for the solute transport models, a general way is to numerically solve the 2D depth-averaged advection-diffusion equations (the 2D ADEs) (Morales-Hernández et al., 2019). Since discontinuities of solutes are commonly seen in floods, numerical difficulties, *i.e.*, numerical diffusion and oscillation, are raised in the presence of the sharp or discontinuous gradient of solute concentration introduced by the non-linear advection terms in the 2D ADEs (Chang and Chang, 2017). Various solute transport models are developed to handle the numerical diffusion and oscillation in different ways, *e.g.*, the finite difference models (Liang et al., 2010), the finite element models (Lee and Seo, 2007), the Lattice Boltzmann models (Ginzburg et al., 2015; Wang et al., 2018), the finite volume models (Morales-Hernández et al., 2019; Zhang et al. 2015), and the meshless approaches such as the Lagrangian approaches (Chang and Chang, 2017; Liu et al., 2020). Specifically, FV-type solute transport models are popularly used due to their effectiveness in simultaneously controlling numerical diffusion and oscillation. Among various FV solute transport models, the Godunov-type FV models with the total variation diminishing (TVD) scheme are found to be satisfactory (Liang, 2010; Lin and Liu, 2019) despite the introduced tedious numerical procedures and heavy computational demands. Nevertheless, numerical diffusion and compression are still unresolved in specific conditions, *e.g.*, in simulating triangle-shaped or trapezoidal-shaped profiles (Hou et al., 2015).

To enhance numerical efficiency, in the last decade, Cellular Automata (CA) framework has been widely adopted by many researchers to establish their efficient models (Chang et al., 2022), because it can solve complex physics through several simple and explicit algebraic equations instead of heavy numerical operators. In addition, CA framework is naturally prone to parallel computing (Chang et al., 2021). For the CA-based shallow water flow models, *e.g.*, the CA flood inundation model (Dottori and Todini, 2011), the CA2D model (Ghimire et al., 2013), the WCA2D model (Guidolin et al., 2016) and the OFS-CA model (Jahanbazi et al., 2017), a set of simple generic transition rules is used to simulate the movement of water instead of numerically solving the 2D SWEs, so that satisfactory efficiency is obtained (Guidolin et al., 2016). Aiming to benefit from the remarkable efficiency of the WCA2D model, Chang et al. (2021) have modified the WCA2D model to

https://doi.org/10.5194/nhess-2024-131
Preprint. Discussion started: 18 September 2024


Natural Hazards and Earth System Sciences Discussions

consider spatial roughness and coupled it with the SWMM as an integrated 2D-1D-1D (overland-gully-sewer) urban inundation model which can finish a real-world simulation with high efficiency. However, all of the aforementioned CA-based models use water levels to determine water movements thus they behave like a non-inertia wave approximation (Caviedes-Voullième et al., 2018), which is inappropriate for simulating flows with strong discontinuities (Costabile et al., 2017; Caviedes-Voullième et al., 2020). To solve this limitation, Chang et al. (2022) have utilized a new framework to build a CA-based shallow water (SWFCA) solver, which explicitly simulates the movement of mass and inertia in a set of simple algebraic equations instead of numerically solving the 2D SWEs like the aforementioned FV models. The Bernoulli hydraulic head is used as the key to link the exchange of mass (water depth) and inertia (water velocity), making the SWFCA solver behave like dynamic waves. Besides, the SWFCA solver preserves the well-balanced property without the need to include special treatment for bed elevation. Through several test cases with regular flows or discontinuous flows, the SWFCA solver has been demonstrated to be as accurate as a Godunov-type first-order FV shallow-water flow model with a popular flux calculation method HLLC (the FV-HLLC model). Specifically, in simulating very shallow flows in very steep slopes, the SWFCA solver is found to be as accurate as the FV-HLLC model with a second-order TVD scheme. In terms of numerical efficiency, the SWFCA solver can be faster than the FV-HLLC model by 1.21-1.28 times. However, such an efficiency is still insufficient for real-world flood inundation applications. Additionally, the SWFCA solver has not yet been parallelized to fully benefit from the natural advantage of CA framework on parallel computing.

On the other hand, for the CA-based solute transport models, so far only Milašinović et al. (2019) have established their weighted cellular automata for pollution transport (CAPT) model to simulate groundwater transported contaminant based on the predicted velocity field from their weighted cellular automata for unsteady groundwater flow (WCAGW) or Darcy's law-based cellular automata for unsteady groundwater flow (MACCA-GW) models. In their CAPT model, the pollutant transport of flow advection and turbulent diffusion mechanisms are simulated by the corresponding set of transition rules that only contain algebraic equations. This model is appropriate and efficient for low Reynold flows, but it cannot be extended to solve solute transport in floods, which is usually in flows with very high Reynold numbers. As a result, Wang et al. (2024) have further developed a CA-based solute transport modeling (STMCA) solver that replaces the tedious numerical operators in solving the 2D-ADEs with a set of simple algebraic equations. The accuracy of the STMCA solver is demonstrated to be the same as a high-accuracy Godunov-type FV model with a TVD scheme (hereinafter referred to as the FV-TVD model) with better efficiency up to 2.90-3.27 times faster than the FV-TVD model. Nevertheless, in certain flows with considerably high Péclet numbers such that flow advection dominates solute transport processes, the STMCA solver and FV-TVD model may both encounter unwanted numerical diffusion and/or compression. Furthermore, the STMCA solver has not been GPU-based parallelized to fully benefit from the inherent nature of CA framework on parallel computing.

To fill this gap, the objective of this study is to develop a CA-based coupled approach for dynamic-wave flow and solute transport simulations. For this goal, the SWFCA solver (Chang et al., 2022) is adopted to simulate dynamic-wave flows. As for the solute transport modeling, the present study extends the research of Wang et al. (2024) to develop a CA-based advanced solute transport (ASTCA) solver with additional procedures to increase the accuracy in flows with high Péclet

https://doi.org/10.5194/nhess-2024-131
Preprint. Discussion started: 18 September 2024


Natural Hazards and Earth System Sciences Discussions

numbers. The SWFCA and ASTCA solvers are coupled to constitute a coupled approach. Furthermore, GPU-based parallelization is implemented on both the two solvers to further enhance the numerical efficiency by OpenCL 2.1 under Nvidia CUDA. The accuracy of the newly proposed ASTCA solver is first verified. Then, the performance of the coupled approach is assessed through three real-world cases involving the simulations of one pluvial and two fluvial floods on real-scale terrains with numerous computational cells. Technical discussion is devoted to the efficiency of the GPU-parallelized coupled approach.

2 Methodology

This study couples the SWFCA solver with a newly proposed ASTCA solver as an effective tool to simulate flood flow and subsequent solute transport. Specifically, the new ASTCA solver utilizes the developed methodology for simulating the flow advection, turbulent diffusion, and material decay transport mechanisms from Wang et al. (2024) with additional treatments to increase the accuracy in high Péclet number flows. In subsect. 2.1, the SWFCA solver is briefly introduced. Next, the new ASTCA solver is introduced in Subsect. 2.2. The coupling methodology for linking the SWFCA and ASTCA solvers is discussed in Subsect. 2.3.

2.1 The CA-based shallow flow (SWFCA) solver of Chang et al. (2022)

The SWFCA solver is proposed to provide a CA-based shallow water flow modeling tool that can behave like dynamic waves. To achieve this goal, the SWFCA solver uses the square-shaped cell to discretize the computational domain into a set of computational cells. Regarding the neighborhood configuration for defining the spatial relation between a computational cell and its surrounding cells, the Von Neumann neighborhood configuration is used in the SWFCA solver. As a result, there are four Von Neumann neighbors at the east, north, west, and south sides of a computational cell. Based on the decided neighborhood configuration, the SWFCA solver uses the Bernoulli hydraulic head as the key factor to determine the water movement so that the coupled relations between water depths and velocities can be reasonably considered. Then, a set of transition rules that consist of five sequential steps to distribute mass (water depths) and inertias (water velocities) from the central cell to its four neighbor cells are incorporated in the SWFCA solver (Chang et al., 2022). In the first step, the SWFCA solver uses the Bernoulli hydraulic heads and mass fluxes to delineate the flow direction and flow condition (either the normal or special flow conditions) of each flow transport route. Then, based on the determined flow direction, the mass flux of a flow transport route is computed by using the Manning and Weir equations in the second step. In the third step, the predicted water depth of each computational cell is decided and is used with the modified energy equation in the fourth step to find the predicted water velocity of each flow transport route. Finally, the SWFCA solver updates the states of each computational cell in the fifth step. After the five steps are executed, the tasks for assigning the boundary conditions and computing the adaptive step based on the Courant-Friedrichs-Lewy (CFL) for the next time marching are performed. For more details on the SWFCA solver, the readers are referred to Chang et al. (2022).

https://doi.org/10.5194/nhess-2024-131
Preprint. Discussion started: 18 September 2024


Natural Hazards and Earth System Sciences Discussions

2.2 The CA-based advanced solute transport (ASTCA) solver

The ASTCA solver is proposed to further increase the accuracy of the STMCA solver in flows with a high Péclet number. For this purpose, the ASTCA solver adopts the same square-shaped cell for discretizing the computational domain as the SWFCA solver. Also, the Von Neumann neighborhood configuration of the SWFCA solver is used in the ASTCA solver according to its convenience for programming and satisfactory accuracy (Chang et al., 2022). The ASTCA solver considers the same solute transport mechanisms as the STMCA solver, *i.e.*, the flow advection, turbulent diffusion, and material decay mechanisms, and they are. These mechanisms are simulated by computing the transported mass leaving/entering each computational cell, which is mathematically described by Eqs. 1 and 2 and conceptually drawn in Fig. 1 by Wang et al. (2024). After the transported mass of the three mechanisms for each cell is determined, the ASTCA solver then updates the solute concentration of each central cell. It is worth mentioning that, in the actual implementation, the solute mass is used instead of the solute concentration for the sake of programming convenience. Finally, the ASTCA solver assigns the boundary conditions and determines the adaptive time step for the next time marching by using the same methodology as the STMCA solver, which can be found in Wang et al. (2024).

2.2.1 Determines the transported mass of the three solute transport mechanisms for each cell

For a central cell, the solute concentrations of the central cell (C_0) and ith neighbor cell (C_1) are first computed by

$$C_0 = M_0/(l^2 d_0) \;\; C_i = M_i/(l^2 d_i) \;\; \forall i \in \{1 \dots 4\} \tag{1}$$

where M_0 and M_i are the solute mass of the central and ith neighbor cells, respectively, d_0 and d_i refer to the water depths of the central and ith neighbor cells, respectively, l is the cell length. In Eq. 1 and the following equations, variables without a superscript are at time *t*. The transported mass of each mechanism is then decided, which is introduced as follows

1. Turbulent diffusion mechanism

In this mechanism, the solutes are actively moved from high concentration to low concentration. Furthermore, a local weight system is incorporated to ensure mass conservation. For a central cell, the solute concentration differences between the central cell and its neighbor cells are first computed by

$$\Delta C_{i,Df} = max(C_0 - C_i, 0) \;\; \forall i \in \{1 \dots 4\} \tag{2}$$

where the subscript *Df* refers to this mechanism. The ith neighbor cell receives transported mass from the central cell if $\Delta C_{i,Df} > 0$. The weight of the ith neighbor cell is decided as

$$W_{i,Df} = \left(D_{0,i}\Delta C_{i,Df}\right) \Big/ \sum D_{0.i}\Delta C_{i,Df} \;\; \forall i \in \{1 \dots 4\} \tag{3}$$

where $D_{0,i}$ is the diffusion coefficient along the direction of the ith neighbor cell. The total transported mass from the central cell to its four neighbor cells at time $t + \Delta t$ is given

https://doi.org/10.5194/nhess-2024-131
Preprint. Discussion started: 18 September 2024


Natural Hazards and Earth System Sciences Discussions

$$I_{tot,Df}^{t+\Delta t} = min\left(\frac{I_{L,Df}}{W_{L,Df}}, \hat{I}_{tot,Df}^{t+\Delta t} + I_{tot,Df}\right) \quad (4)$$

where the subscript $\boldsymbol{L}$ refers to the index of the neighbor cell with the maximum weight, $W_{\boldsymbol{L},Df}$ is the maximum weight, $I_{\boldsymbol{L},Df}$ is the transported mass to the neighbor cell with the maximum weight ($= D_{0,\boldsymbol{L}}\Delta C_{\boldsymbol{L},Df} d_0 \Delta t$) with Δt is the adaptive time step, $\hat{I}_{tot,Df}^{t+\Delta t}$ refers to the maximum value of total transported mass that will not cause artificial oscillation, $I_{tot,Df}$ is the total transported mass at the previous time stage. $\hat{I}_{tot,Df}^{t+\Delta t}$ is determined as

$$\hat{I}_{tot,Df}^{t+\Delta t} = l^2 min\left(\frac{\Delta C_{i,Df}|^{\Delta C_{i,Df}>\tau}}{\frac{W_{i,Df}}{d_i}+\frac{1}{d_0}}\right) \ \forall i \in \{1 \dots 4\} \quad (5)$$

where τ refers to a small tolerance (=10^{-8} in the present manuscript). After $I_{tot,Df}^{t+\Delta t}$ is computed, the transported mass to the ith neighbor cell is decided by

$$I_{i,Df}^{t+\Delta t} = W_{i,Df} I_{tot,Df}^{t+\Delta t} \ \forall i \in \{1 \dots 4\} \quad (6)$$

2. Flow advection mechanism

In this mechanism, the solute is passively moved according to the velocity field. Consequently, the transported mass to the ith neighbor cell is written as

$$I_{i,Adv}^{t+\Delta t} = max\left(\Theta_{(0,i)} q_{0,i}^{t+\Delta t}, 0\right) C_{0,i} \Delta t \times l \quad (7)$$

where the subscript *Adv* represents the flow advection mechanism, $q_{0,i}^{t+\Delta t}$ is the computed unit-width discharge at the ith cell edge from the SWFCA solver at the time $t + \Delta t$, $C_{0,i}$ is the solute concentration at the cell edge, and $\Theta_{(0,i)}$ is an internal variable for checking $q_{0,i}^{t+\Delta t}$ is toward the cell edge ($\Theta_{(0,1)} = 1$, $\Theta_{(0,2)} = 1$, $\Theta_{(0,3)} = -1$, and $\Theta_{(0,4)} = -1$). The ASTCA solver also introduces the use of the flux limiter to formulate $C_{0,i}$. Taking $C_{0,1}$ and $C_{0,3}$ as an example, they are given by

$$C_{0,1} = C_0 + 0.5l \times S_{0,1} \ \ C_{0,3} = C_0 - 0.5l \times S_{0,3} \quad (8)$$

$$S_{0,1} = S_{0,3} = \frac{1}{l}\phi\left(r_{0,1\leftrightarrow 3}\right)(C_1 - C_0) \quad (9)$$

$$r_{0,1\leftrightarrow 3} = \frac{C_0 - C_3}{C_1 - C_0} \quad (10)$$

with $\phi(r)$ is the flux limiter. In the proposed ASTCA solver, the Superbee flux limiter is selected as the flux limiter because of its recognized accuracy. Nevertheless, numerical compression that will distort the simulated profile is found to emerge in flows with a high Péclet number (Hou et al., 2015). The reason for this distortion is related to the underestimation and overestimation of the transported mass, which will subsequently make the Superbee flux limiter tend to smoothen the concentration profile segments with relatively steeper slopes and sharpen the concentration profile segments with relatively milder slopes (Hou et al., 2015). Such a numerical difficulty can occur when simulating triangle-shaped, trapezoidal-shaped,

https://doi.org/10.5194/nhess-2024-131
Preprint. Discussion started: 18 September 2024


Natural Hazards and Earth System Sciences Discussions

or Gaussian-shaped profiles, as extensively studied by Hou et al. (Hou et al., 2015). As drawn in Fig. 2a, the transported mass through the 1st cell edge by Eq. 7 with a value of $\left|q_{0,1}^{t+\Delta t}\right| C_{0,1}\Delta t \times l$ (the gray area at the 1st cell edge) is underestimated as the actual transported mass should be the green trapezoidal area. Thus, $C_{0,1}$ is adjusted to be a mean value as $C_{0,1} = \left(C_{0,1} + C'_{0,1}\right)/2$ where $C'_{0,1}$ is estimated by the unit-width discharge at the 1st cell edge, and the piecewise slope and water depth of the central cell. A general form for adjusting $C_{0,i}$ is given by

$$C_{0,i} = C_{0,i} - \Theta_{(0,i)} 0.5 S_{0,i} \times \frac{|q_{0,i}|\Delta t}{d_0} \tag{11}$$

if and only if $I_{i,Adv}^{t+\Delta t} > 0$. It is worth mentioning that $C_{0,i}$ could produce false diffusion at the tail and front of a moving concentration profile, particularly the rectangle-shaped profile, in steady flows. The false diffusion is related to the fact that the well-mixed assumption of solute is no longer guaranteed when flows are in a steady state. To mitigate this false diffusion, taking the central cell and its 1st cell edge in Fig. 2b as an example, the ASTCA solver computes the upstream and downstream bounds of $C_{0,1}$ as $C_{0,1}^{us} = \left(5C_3 - C_{3,3}\right)/2$ and $C_{0,1}^{ds} = \left(3C_1 - C_{1,1}\right)/2$, respectively, to include the spatial tendency of the profile in the adjustment. Then, if the central cell is at the profile front (*i.e.*, $C_3 > 0$ and $C_1 = 0$), $C_{0,1}$ will be set as $C_{0,1}^{ds}$ if $C_{0,1} < \delta \times C_{0,1}^{ds}$ to express the condition that the profile front has not touched the cell edge. If the central cell is at the profile tail (*i.e.*, $C_3 = 0$ and $C_1 > 0$), $C_{0,1}$ is conversely enlarged to be $\max\left(\delta C_{0,1}^{ds}, C_{0,1}\right)$ to represent the condition that the solute concentration of the central cell is underestimated. In the present study, δ is computed by an empirical formula of $0.95 - 1000\left(D_{0,i}\Delta C_{i,Df}\right)/\left(C_{0,i} l \left|q_{0,i}^{t+\Delta t}\right|/d_0\right)$ by the present study to account for the relative strength between the turbulent diffusion and flow advection.

3. Turbulent diffusion mechanism

The decreased mass due to this mechanism is estimated by

$$I_{tot,Decay}^{t+\Delta t} = \Delta t \times k[C_0]^N \times (l^2 d_0) \tag{12}$$

where *k* and *N* are the temporal decay rate and order of the reaction, respectively.

After the transported mass of the three mechanisms is computed, a simple mass conservation check is performed to avoid the occurrence of negative solute mass. The summed transported mass is first computed as $I_{tot}^{t+\Delta t} = \sum_{i=1}^{4}\left(I_{i,Adv}^{t+\Delta t} + I_{i,Df}^{t+\Delta t}\right) + I_{tot,Decay}^{t+\Delta t}$ and compared with M_0. If $M_0 < I_{tot}^{t+\Delta t}$, $I_{i,Df}^{t+\Delta t}$, $I_{i,Adv}^{t+\Delta t}$, and $I_{i,Decay}^{t+\Delta t}$ are all multiplied by $M_0/I_{tot}^{t+\Delta t}$.

2.2.2 Update the solute mass of each cell

The solute mass of each central cell is updated by a simple equation as

$$M_0^{t+\Delta t} = M_0 - \sum_{i=1}^{4}\left(I_{i,Adv}^{t+\Delta t} + I_{i,Df}^{t+\Delta t}\right) - I_{tot,Decay}^{t+\Delta t} \tag{13}$$

with $M_0^{t+\Delta t}$ is the updated solute mass of the central cell.

https://doi.org/10.5194/nhess-2024-131
Preprint. Discussion started: 18 September 2024

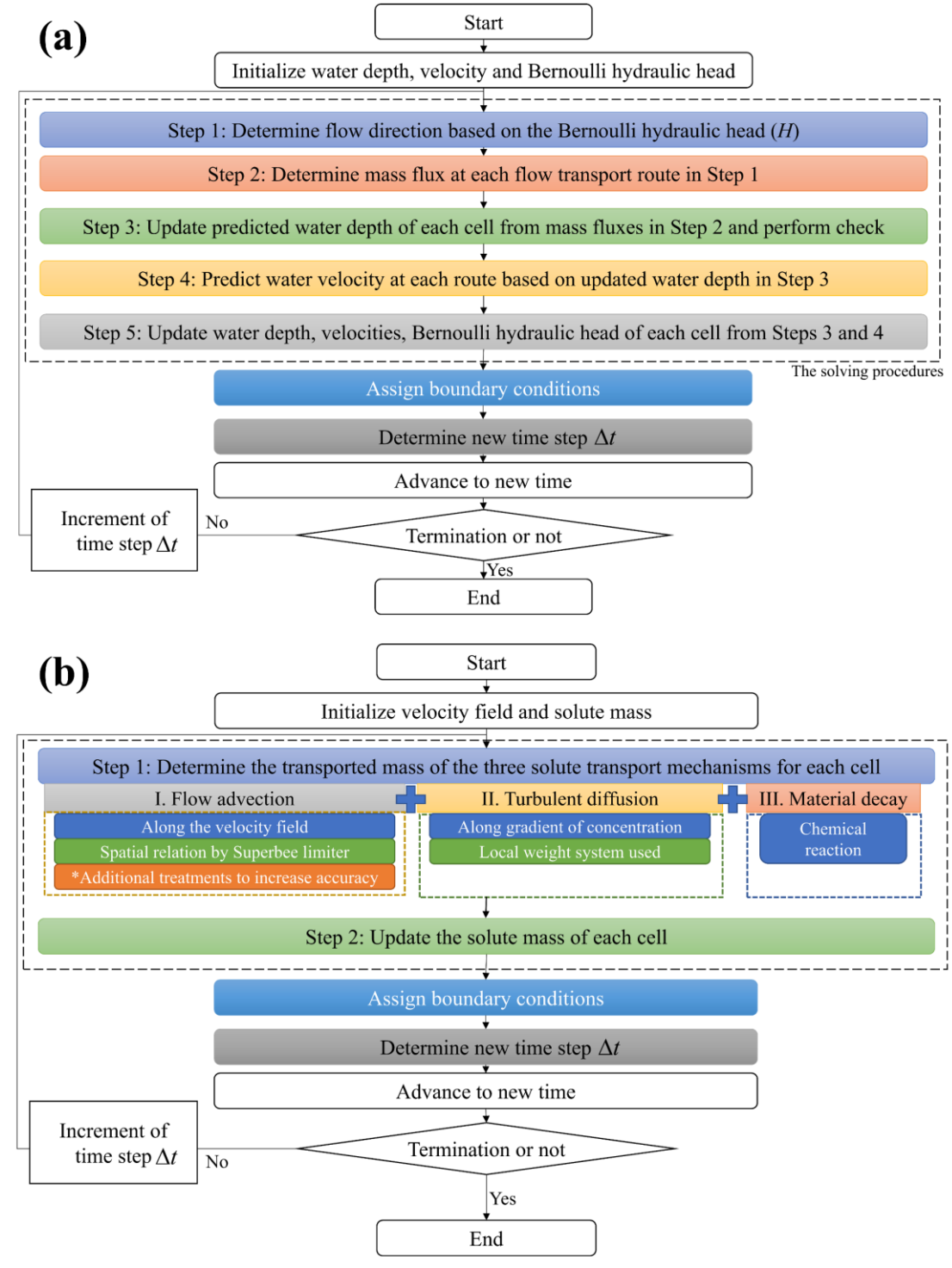

Figure 1: The flowcharts of the (a) SWFCA and (b) ASTCA solvers, respectively.

https://doi.org/10.5194/nhess-2024-131
Preprint. Discussion started: 18 September 2024

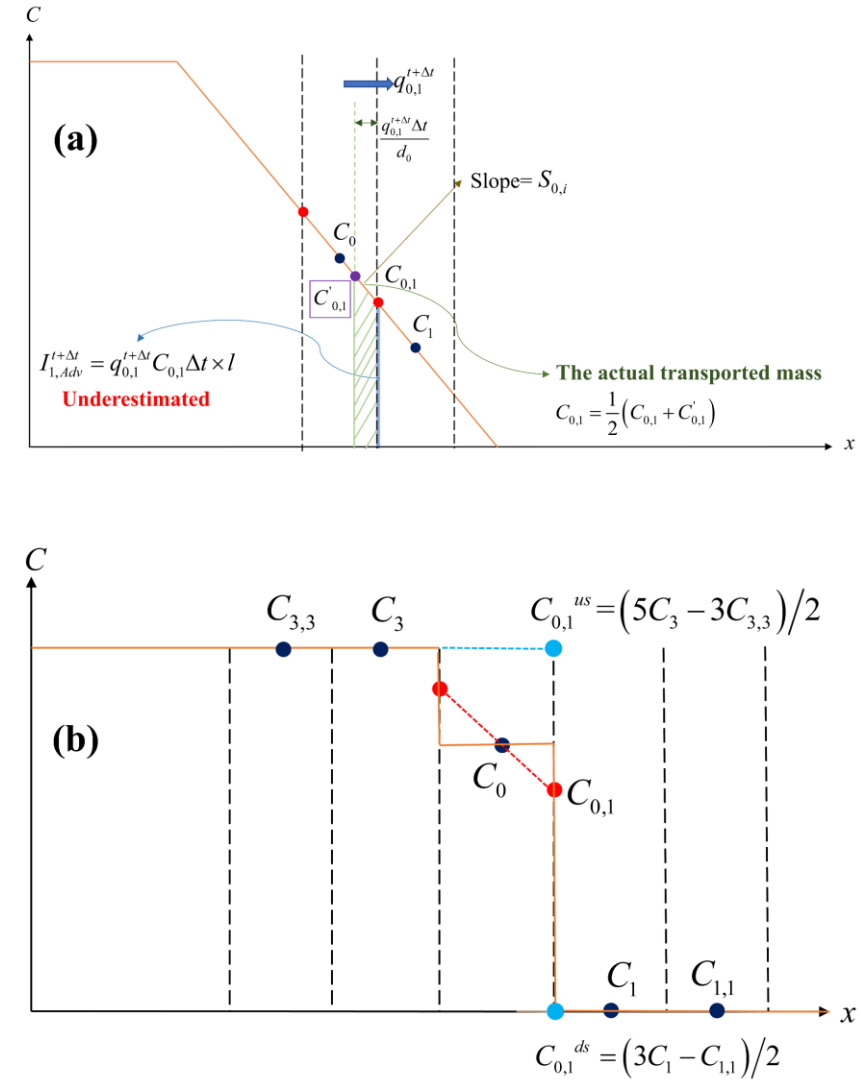

Figure 2: The schematic illustrations of the additional treatments of the ASTCA solver to increase the accuracy in high Péclet number flows. The treatments for (a) numerical compression and (b) numerical diffusion, respectively.

2.3 The coupling methodology between the SWFCA and ASTCA solvers

The SWFCA and ASTCA solvers are completely coupled in the same program to avoid unnecessary variable exchange between the two solvers. The execution of the two solvers is sequential, *i.e.*, the ASTCA solver is executed after the SWFCA solver is performed since the ASTCA solver requires the predicted transport mass fluxes to conduct the simulation. The flowchart of the proposed CA-based coupled approach is drawn in Fig. 3a. As this figure displays, the coupled approach will first call the SWFCA solver to execute its five sequential steps to compute the updated velocity field. Then, the boundary conditions are assigned, and the ASTCA solver is commanded to determine the transported mass of the three solute transport

https://doi.org/10.5194/nhess-2024-131
Preprint. Discussion started: 18 September 2024


Natural Hazards and Earth System Sciences Discussions

mechanisms. The ASTCA solver then computes the new solute mass based on the determined transported mass of solutes. Then, the boundary conditions of the ASTCA solver are assigned. After that, the global-wised adaptive time step for the two solvers is determined under the CFL and diffusion conditions. The present approach then moves into the next time marching until the simulation is finished.

As the SWFCA and ASTCA solvers will be GPU-parallelized, it is essential to count the number of loops that would be needed to parallelize (Yu and Chang, 2023). As displayed in Fig. 3a, for the SWFCA solver, there is one main loop for the first and second steps. The third step incorporates a main loop to compute the predicted water depth of each computational cell, and another main loop to check whether the delineated flow directions in the first step are unchanged with the predicted water depth. Next, both the fourth and fifth steps require one main loop. As to the assignment of the boundary conditions, there is a relatively small loop introduced. As for the ASTCA solver, there is a main loop to compute the transported mass of the three mechanisms for each cell, and a main loop to update the solute mass of each cell. Then, there is a relatively small loop for assigning the boundary conditions. Hence, there are eight main loops and two relatively small loops for the proposed approach. Totally, there are ten loops.

3 The GPU parallelization of the SWFCA and ASTCA solvers

In GPU-based parallelization, the executions of the described computing procedures in Subsects. 2.1 and 2.2 are applied on GPUs instead of sequentially on the CPU since GPUs can provide satisfactory enlargement of efficiency without the use of high-performance computing equipment (Dazzi et al., 2018; Sanders and Schubert, 2019; Yu and Chang, 2023). Given that the SWFCA solver is programmed in C++, the newly developed ASTCA solver is also written in C++ to maintain consistency between the two solvers. Furthermore, the API of OpenCL 2.1 under the Nvidia CUDA (Compute Unified Device Architecture) is used to write the GPU-parallelized SWFCA and ASTCA solvers so that they can benefit from the remarkable portability of OpenCL. The details for implementing GPU parallelization on the SWFCA and ASTCA solvers are introduced in Subsects. 3.1 and 3.2, respectively.

3.1 The GPU parallelization of the SWFCA solver

In the SWFCA solver, the states of each computational cell (*i.e.*, the Bernoulli hydraulic head, water depths, and water velocities) and the states of each cell edge (*i.e.*, unit-width discharges and mass fluxes) are stored in their corresponding 1D arrays. Equivalently speaking, GPU parallelization is to let the computations of these 1D arrays in a loop be executed parallelly on GPUs. In the OpenCL structure, the parallelization is undertaken by executing kernel functions with variables in the virtual OpenCL workspace. Since the allocated variables in the virtual OpenCL workspace cannot be directly accessed by the main thread in the CPU, it is essential to lower the time-consuming readings/writings of variables between the main thread and the virtual OpenCL workspace. Correspondingly, to implement the GPU-based parallelization on the SWFCA solver, the aforementioned state variables of any central cell and any cell edge are all allocated in the OpenCL workspace.

https://doi.org/10.5194/nhess-2024-131
Preprint. Discussion started: 18 September 2024


Natural Hazards and Earth System Sciences Discussions

Furthermore, when executing the kernel functions, the local sizes for specifying the size of a work-group instance (*i.e.*, the block) for the *enqueueNDRangeKernel* function are filled with *NULLRange*. In this way, the OpenCL implementation will determine the appropriate work-group instances dynamically.

In the aspects of the actual GPU implementation, the whole flowchart of the GPU-parallelized proposed approach is drawn in Fig. 3b for illustration. At the beginning of a simulation, the main thread will call the SWFCA solver to allocate the required state variables in the virtual OpenCL workspace. Input data is read and sent into the virtual OpenCL workspace for initialization. At each time stage, the computations of the five main loops are performed by sequentially executing the five kernel functions. As to the task of assigning the boundary conditions, it is moved and combined with the task of determining the new adaptive time step since the number of the boundary cells is often much less than the number of computational cells. An additional state variable is correspondingly incorporated with values of 1 as the SWFCA solver's boundary cell and 0 as the other cell to merge these two tasks. The merged two tasks will introduce a main loop to compute the adaptive time step of a central cell and assign the corresponding boundary condition if the central cell is marked as the SWFCA solver's boundary cell. A reduction operator is incorporated to find the minimum value of the adaptive time steps. Furthermore, as drawn in Fig. 3b, the task for assigning the boundary conditions in the ASTCA solver is merged with that of the SWFCA solver, which will be introduced in the next subsection.

3.2 The GPU parallelization of the ASTCA solver

The ASTCA solver is GPU-parallelized by using the identical parallelization implementation of the SWFCA solver. The state variables in the ASTCA solver, *i.e.*, solute mass and turbulent diffusion coefficients of each computational cell, and mass flux across the cell edge, are all allocated in the virtual OpenCL workspace. The computations of the two sequential steps of the ASTCA solver are applied on GPUs by executing two corresponding kernel functions, as Fig. 3b displays. Regarding the size of a work-group instance in executing the two kernel functions, the ASTCA solver also lets the OpenCL implementation dynamically decide it. As previously mentioned in Subsect. 3.1, the task for assigning the boundary conditions is moved and merged with that of the SWFCA solver. A value of 2 is added to the state variable of the SWFCA solver that is used for identifying the SWFCA solver's boundary cell (a value of 1) to represent the ASTCA solver's boundary cell. With this treatment, the number of loops to be parallelized in the GPU-parallelized proposed approach is eight, which is less than the original proposed approach (ten in total).

4 Model verification

In this section, the accuracy of the proposed CA-based coupled approach is investigated through four test cases. Since the accuracy of the SWFCA solver has already been demonstrated to be satisfactory (Chang et al., 2022), only the accuracy of the ASTCA solver is herein verified and compared with the STMCA solver of Wang et al. (2024) and the state-of-the-art FV-TVD model of Liang (2010). The selected FV-TVD model is coupled with a widely used FV-HLLC model as a FV-

https://doi.org/10.5194/nhess-2024-131
Preprint. Discussion started: 18 September 2024

Natural Hazards and Earth System Sciences
Discussions

based coupled approach for the rest analysis by a similar mean as the proposed CA approach. As for the STMCA solver, it uses the simulated results of the FV-HLLC model to perform its solute transport computation.

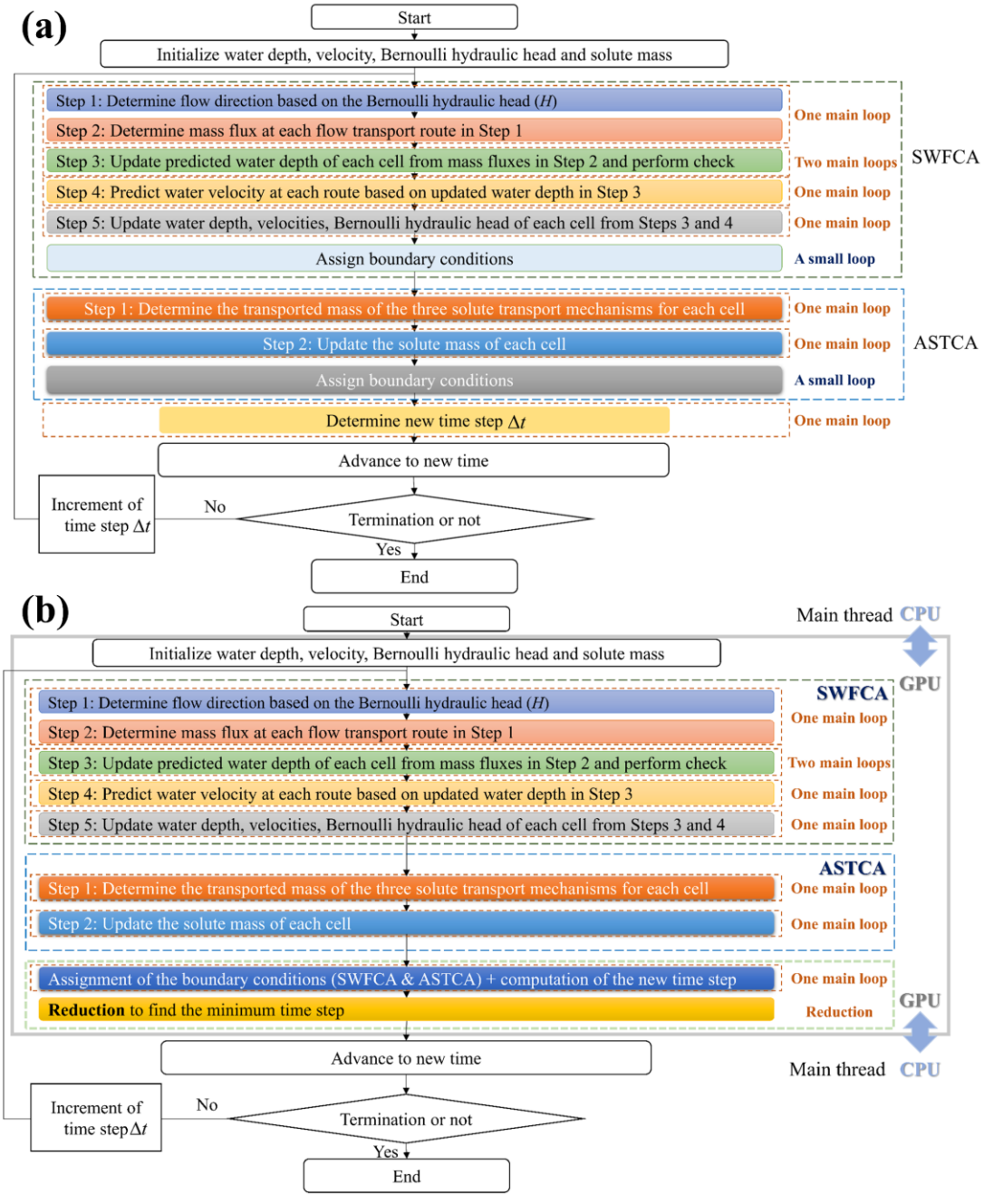

Figure 3: (a) The flowchart of the SWFASTCA approach. The number of the main loops that scan over each computational cell and the number of the small loops for assigning the boundary conditions are both marked. (b) The flowchart of the GPU-parallelized CA-based approach. The readings/writings between the main thread (CPU) and virtual OpenCL workspace (GPU) are drawn in the figure.

https://doi.org/10.5194/nhess-2024-131
Preprint. Discussion started: 18 September 2024


Natural Hazards and Earth System Sciences Discussions

4.1 Case 1: solute transport in a 2D uniform velocity field (movement of solutes with steep gradients in a 2D steady uniform flow)

Case 1 simulates the solute transport with concentration discontinuities in a horizontal and frictionless channel that has a length of 10,000 m and a width of 10 m (Chang and Chang, 2017). A uniform water depth of 0.5 m and water velocities as u=0.7 m/s and v=0 m/s are given for the velocity field. The left and right edges of the computational domain are both prescribed as the transmissive boundary. In such a way, the released solutes will be passively moved by the specified velocity field only along the x direction. The computational domain is discretized by a square cell with a length of 2 m, resulting in 25,000 computational cells. As for the concentration field, there are four scenarios herein. For the first two scenarios, the initial solute concentration profile is given as a rectangle-shaped profile (*i.e.*, top hat tracer) with a concentration of 1 kg/m^3 within $|x - 400| \leq 800$ m. The time-invariant and uniform diffusion coefficient for the first scenario is given as 0 m^2/s so that an infinite Péclet number is introduced. As a result, the first scenario is in the advection-dominated condition. As for the second scenario, the diffusion coefficient is given as 10 m^2/s to let this scenario be in the diffusion-dominated condition. For the third scenario, the initial solute concentration profile is a triangle-shaped profile along the x direction with its center at x=800 m, a base length of 800 m, and a peak concentration of 1 kg/m^3. In the fourth scenario, a trapezoidal-shaped profile with its center at x=800 m, a top length of 80 m, a base length of 600 m, and a peak concentration of 1 kg/m^3 is used to define the initial solute concentration profile. The diffusion coefficients in the last two scenarios are both given as 0 m^2/s. Therefore, the first, third, and fourth scenarios are all in the advection-dominated condition. The simulation durations of the four scenarios are all 9000 s to observe the movement of the solute, and the L_2 norm of solute concentration is computed by taking all the simulated solute concentrations in the computational domain at this time. The analytical solutions in the advection-dominated scenarios are straightforward to derive since these scenarios are all in the pure advection condition. As to the diffusion-dominated scenario, the analytical solution by Tian et al. (2022) is used.

The simulated results of the ASTCA solver, STMCA solver, and FV-TVD model at t=9000 s in the four scenarios are drawn in Figs. 4a-4d, respectively. The analytical solutions are also included in these figures for reference. Inspection from these figures reveals that the STMCA solver and FV-TVD model produce almost identical results in all scenarios. As to the ASTCA solver, its accuracy is found to be higher than the STMCA solver and FV-TVD model in advection-dominated scenarios. In the first scenario, the ASTCA solver successfully mitigates the unwanted numerical diffusions near the fronts and tails that are seen in the STMCA solver and FV-TVD model (Fig. 4a). As for the third and fourth scenarios (drawn in Figs. 4c and 4d, respectively), both the STMCA solver and FV-TVD model give distorted results because of the numerical compression. Conversely, the ASTCA solver produces results that agree with the analytical solutions well. In the second scenario, the ASTCA solver, STMCA solver, and FV-TVD model give very similar results that all match the analytical solutions well. The L_2 norms of solute concentrations are computed and listed in Table 1. From this table, it is found that the accuracy of the STMCA solver and FV-TVD model is almost identical. As to the ASTCA solver, it outperforms the STMCA solver and FV-TVD model in all four scenarios. It is worth mentioning that the ASTCA solver still has better performance

https://doi.org/10.5194/nhess-2024-131
Preprint. Discussion started: 18 September 2024


Natural Hazards and Earth System Sciences Discussions

than the STMCA solver and FV-TVD model in the diffusion-dominated scenario, which means that the inclusion of the additional treatments for mitigating unwanted numerical diffusion and compression is meaningful and effective even in the diffusion-dominated condition. Thus, based on Figs. 4a-4d and Table 1, the STMCA solver is verified to have the same accuracy as the FV-TVD model. As for the proposed ASTCA solver, it outperforms the STMCA solver and FV-TVD model in both the advection-dominated and diffusion-dominated scenarios, particularly in the advection-dominated scenarios where significant accuracy enhancement is seen. Additionally, it is deduced that the accuracy enhancement becomes less when the diffusion begins to dominate.

4.2 Case 2: solute transport in a 2D rotating velocity field (transport of Gaussian-shaped solutes with steep gradients in a 2D steady rotating flow)

Case 2 considers a rotating velocity field of Liu et al. (2020) since the circulation phenomenon is commonly seen in river and overland flows. Also, this kind of rotating velocity field is recognized to be difficult for mesh-based models so it is used to test our proposed ASTCA solver (Liu et al., 2020). The corresponding solute transports are thus along both the *x* and *y* directions. The computational domain is a frictionless and horizontal square-shaped plate with a length of 3400 m. A uniform water depth of 1.0 m is prescribed for the velocity field. The water velocities of the counter-clockwise velocity field are specified as $u = -0.001\pi(y - 1700)$ m/s and $v = 0.001\pi(x - 1700)$ m/s, meaning one rotation takes 2000 s. As to the boundary condition, all of the four edges are set as the transmissive boundary. A square cell with a length of 4 m is adopted to discretize the computational domain into 724,201 cells. The concentration field is a Gaussian-shaped concentration profile as

$$C(x, y, t) = exp\left(-\frac{(x-x_o(t))^2}{2\sigma_x^2} - \frac{(y-y_o(t))^2}{2\sigma_y^2}\right) \quad (14)$$

where σ_x and σ_y are the variance in the *x* and *y* directions, respectively, $x_o(t)$ and $y_o(t)$ refer to the center of the Gaussian-shaped profile. In the present study, $\sigma_x = \sigma_y = 200$ m. Initially, the center of the Gaussian-shaped profile is located at (900 m, 1700 m). The simulation duration is given as 2000 s to see the simulated profile after one rotation. The L_2 norm of solute concentration is computed by using the simulated profile at 2000 s.

The analytical and simulated solute concentration profiles after one rotation (*t*=2000 s) along the lines *x*= 900 m and *y*= 1700 m are respectively drawn in Figs. 5a and 5b. From these two figures, the STMCA solver and FV-TVD model provide almost identical results. However, both the two solute concentration profiles have a spuriously flat area near the center. Such a distortion can still be found in the ASTCA solver but with a much less magnitude. The L_2 norm of solute concentrations is computed and listed in Table 1. Inspection from Table 1 reveals that the accuracy of the STMCA solver is the same as the FV-TVD model, and the accuracy of the ASTCA solver is significantly higher than the other two. Hence, based on Figs. 5a-5b and Table 1, the ASTCA solver has proven its ability to provide more reliable results than the state-of-the-art FV-TVD

https://doi.org/10.5194/nhess-2024-131
Preprint. Discussion started: 18 September 2024

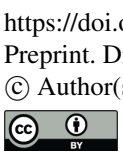

Natural Hazards and Earth System Sciences
Discussions

model in a 2D rotating velocity field. The additional treatments for increasing the accuracy are proven to be effective in more complex flow conditions.

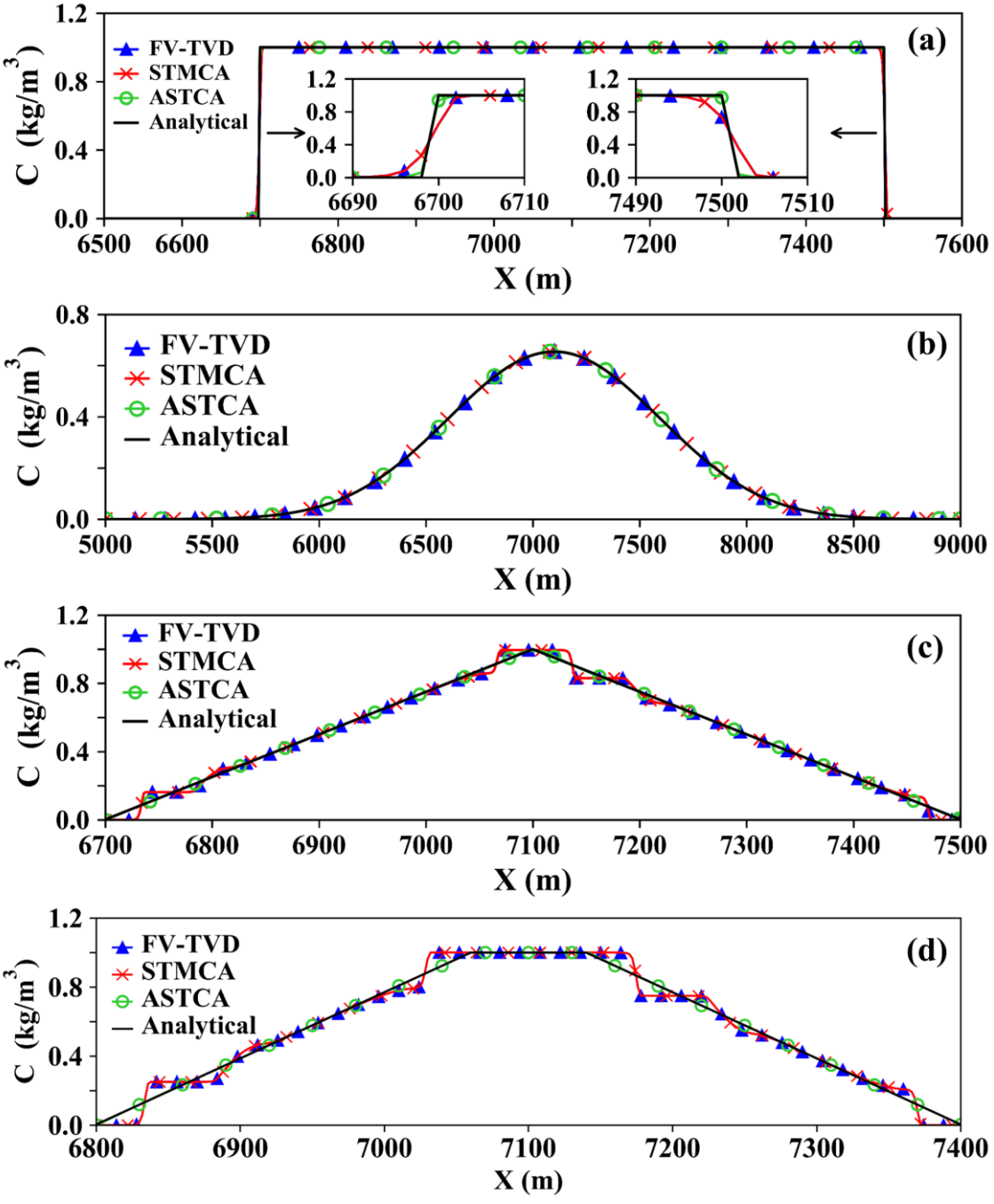

Figure 4: Model verification Case 1. The comparison of the analytical and simulated results when *t*=9000 s. The rectangle-shaped profiles with (a) D=0 m²/s and (b) D=10 m²/s. (c) The triangle-shaped profile with D=0 m²/s. (d) The trapezoidal-shaped profile with D=0 m²/s.

https://doi.org/10.5194/nhess-2024-131
Preprint. Discussion started: 18 September 2024

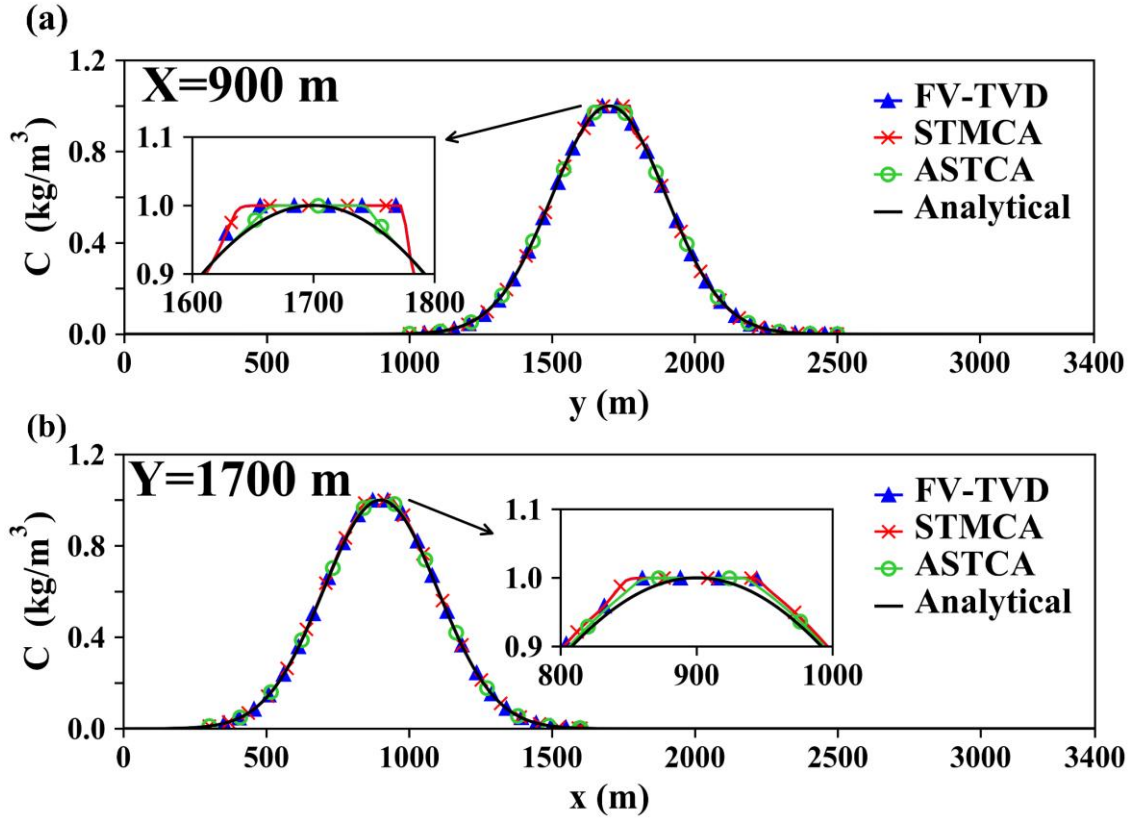

Figure 5: Model verification Case 2. The solute concentration profiles along (a) *x*= 900 m and (b) *y*=1700 m of the ASTCA solver, STMCA solver, and FV-TVD model after one rotation (*t*=2000 s).

Table 1: The comparison of the numerical accuracy among the proposed ASTCA solver, STMCA solver, and FV-TVD model in Cases 1-2 of the model verification.

Case	Scenarios	The ASTCA solver L_2 norm	The STMCA solver L_2 norm	The FV-TVD model L_2 norm
1	Rectangle-shaped profile with D=0 m^2/s	0.00502	0.03166	0.03166
	Rectangle-shaped profile with D=10 m^2/s	0.00228	0.00248	0.00248
	Triangle-shaped profile with D=0 m^2/s	0.00364	0.04090	0.04090
	Trapezoidal-shaped profile with D=0 m^2/s	0.00204	0.07928	0.07928
2		0.00485	0.01207	0.01207

https://doi.org/10.5194/nhess-2024-131
Preprint. Discussion started: 18 September 2024


Natural Hazards and Earth System Sciences Discussions

4.3 Case 3: solute transport in a 2D dambreak flows over a triangular bump with various boundary conditions (discontinuous solute concentrations in dambreak flows over a complex terrain with various boundary conditions)

In Case 3, solute transport in unsteady dambreak flows is involved to check the ASTCA solver. This dambreak flow case originates from the CADAM project and is extensively used to discover the ability of a shallow water flow model to handle partially reflective waves, hydraulic jumps/drops, and wet-dry interfaces (Chang et al., 2011; Kao and Chang, 2012). The computational domain comprises a reservoir with a length of 15.5m and a width of 1.0 m, a rectangular rough channel with a length of 22.5 m and a width of 1.0 m. A gate is placed at the downstream end of the reservoir where x=15.5 m. A triangular bump with a length of 6.0 m and a height of 0.4 m is located between 22.5 m and 34.5 m. All of the bed elevations except for the triangular bump are zero. The Manning roughness coefficient is specified as 0.0125 s/m$^{1/3}$. Details of the configuration of this case can be found in Chang et al. (2022). Similar to Chang et al. (2022), the first and second scenarios of this CADAM project are selected for Case 3, *i.e.*, the first scenario with the dry bed condition and the open end, and the second scenario with the wet bed condition and the closed end. The computational domain is discretized by square cells with a length of 0.1 m into 4,411 cells. The initial solute concentration profiles for the two scenarios are both the trapezoidal-shaped profile with the center at x=14.5 m, top length of 1 m, base length of 2 m, and peak concentration of 1 kg/m^3. The simulation durations of the two scenarios are both 40 s. The analytical solution for solute concentration is absent in this case. The comparison among the ASTCA solver, STMCA solver, and FV-TVD model is conducted by taking the simulated concentration profiles at t=7.0 s and 8.1 s for the sake of demonstration.

The three simulated concentration profiles at t=7.0 s and 8.1 s in the two scenarios are respectively drawn in Figs. 6a and 6b. From the two figures, it is found that at two times, the ASTCA solver, STMCA solver, and FV-TVD model produce very similar concentration profiles despite the latter two simulating relatively bent curves at the tail and front of the profiles because of unwanted numerical diffusion/compression. The ASTCA solver successfully maintains straight lines near the tail and front of the profiles at both two times in both of the two scenarios. Correspondingly, the accuracy of the STMCA solver is the same as the FV-TVD model. The ASTCA solver can provide more physically reliable simulated results than the STMCA solver and FV-TVD model. Thus, the ASTCA solver has better performance than the STMCA solver and FV-TVD model in simulating solute transport in dambreak flows.

4.4 Case 4: solute transport in a pluvial flood on a real-scale terrain

Case 4 includes the solute transport in a pluvial flood event on a real-scale terrain in Taiwan. The terrain used by Wang et al. (2024) for their model applications and efficiency assessment is selected for Case 4. This study site is located in the southern region of Taiwan, as Fig. 6a of Wang et al. (2024) depicts. The corresponding terrain is in the downstream part of the Dianbo River catchment (depicted in Fig. 6a of Wang et al. (2024)) and has a 10-year return period flood levee along the Dianbo River mainstream, as drawn in Fig. 6b of Wang et al. (2024). The present study uses the same land use (Fig. 6c of Wang et al. (2024)) and specification of the “pollutant release” regions (Fig. 6d of Wang et al. (2024)) for releasing pollutants. The used

https://doi.org/10.5194/nhess-2024-131
Preprint. Discussion started: 18 September 2024

Natural Hazards and Earth System Sciences
Discussions

DEM has 28,743 cells with a length of 20 m. The sewer networks are ignored as the focus is not on the overland flow modeling.

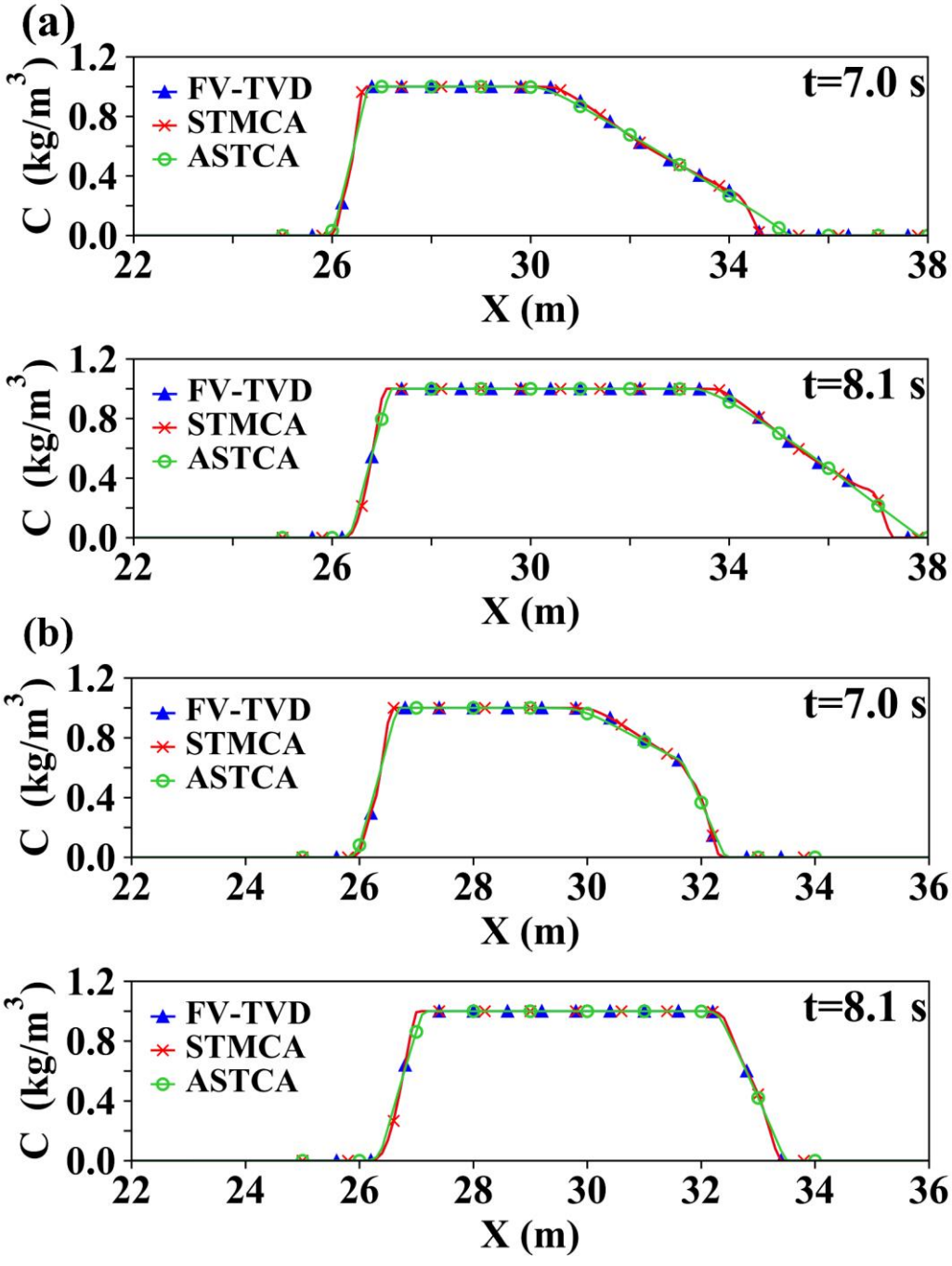

Figure 6: Model verification Case 3. The comparison in simulated solute concentration profiles among the ASTCA solver, STMCA solver, and FV-TVD model when *t*=7.0 s and 8.1 s in the (a) first and (b) second scenarios.

https://doi.org/10.5194/nhess-2024-131
Preprint. Discussion started: 18 September 2024


Natural Hazards and Earth System Sciences
Discussions

To introduce a pluvial flood on this study site, the used rainfall data of a historical 23 August 2018 event by Wang et al. (2024) is utilized again, as drawn in Fig. 6e of Wang et al. (2024). The simulation duration is given as 24 hours to let the overland flows recede. The pollutants will be released from the "pollutant release" regions once the water depth of a cell in the regions exceeds 0.3 m. The pollutants are released in an initial concentration of 1000 ppm and a first-order decay rate k of 0.02 1/hr. Finally, the diffusion coefficients are computed by using the proposed formulas that include the consideration of longitudinal dispersion and turbulent diffusion (Liang et al., 2010). The comparison in accuracy is conducted by examining the solute concentration map and the predicted solute concentration hydrographs in two observed points (locations are the same as in Wang et al. (2024), see Fig. 6d for illustration). For more details, the readers are referred to Wang et al. (2024).

The solute concentration maps of the ASTCA solver, STMCA solver, and FV-TVD model are drawn in Fig. 7a for comparison. The "*pollutant releases*" regions are also drawn in this figure. Apparently, the three solute concentration maps are almost the same and reasonable. The solute concentration hydrographs at the observed points P1 and P2 are drawn in Figs. 7b and 7c, respectively. It is found that, at each observed point, the STMCA solver gives almost the same result as the FV-TVD model. The result of the ASTCA solver is quite similar to those of the STMCA solver and FV-TVD model despite the latter two both introducing some minor variations near the peaks of the hydrographs. This finding is related to the fact that the ASTCA solver has additional treatments to provide better estimations of the transported mass. Thus, although the results are almost the same, the results of the ASTCA solver are relatively more reliable than the STMCA solver and FV-TVD model.

5 Model efficiency assessment

The efficiency of the original and GPU-parallelized CA-based coupled approaches for various flood flows and subsequent solute transport in real-world flood events is evaluated through three selected cases (Cases A-C). Basically, many serious flooding events in recent years are either pluvial flooding due to heavy rainfall or fluvial flooding because of overtopping rivers. Therefore, the present study adopts several pluvial and fluvial flooding events to test our proposed approach. Case A considers the solute transport in a fluvial flood event due to serious dambreak flows toward buildings. Cases B and C respectively simulate pollutant events in pluvial and fluvial flood events on a real-world terrain in Taiwan. In each case, there are normal and fine grid systems for the assessment. Hence, there are totally six scenarios. To make a fair assessment, the FV-based, CA-based, and GPU-parallelized CA-based approaches are programmed based on the same structure. All of the simulations are conducted on an Intel (R) Core (TM) i9 PC equipped with 6.0 GB RAM and a core of 3.4 GHz clock speed. The equipped graphic card is an Intel (R) UHD Graphics 630 graphic card.

https://doi.org/10.5194/nhess-2024-131
Preprint. Discussion started: 18 September 2024

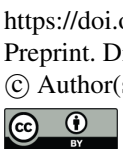

Natural Hazards and Earth System Sciences
Discussions

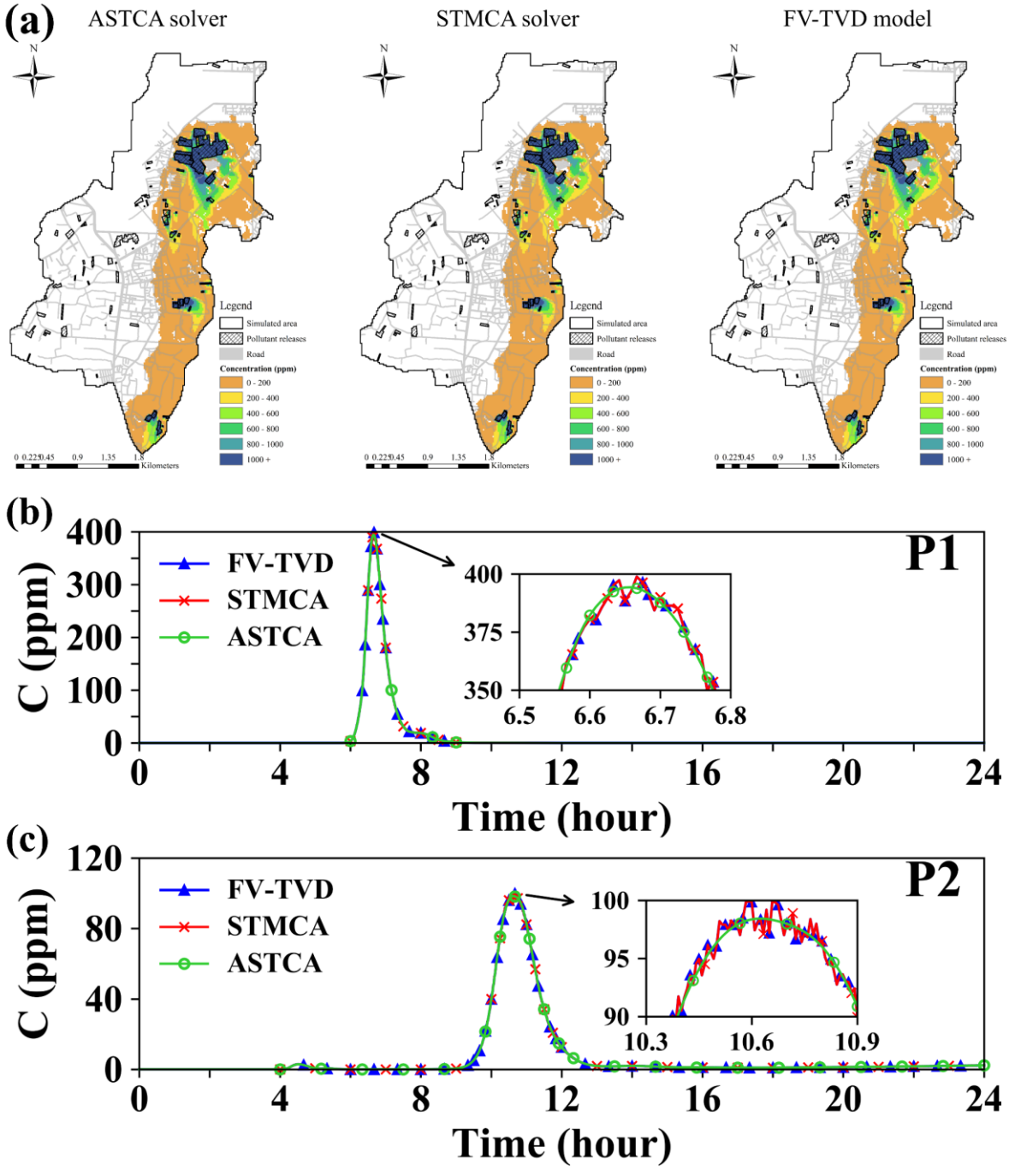

Figure 7: Model verification Case 4. (a) The solute concentration maps of the ASTCA solver, STMCA solver, and FV-TVD model. The solute concentration hydrographs of the ASTCA solver, STMCA solver, and FV-TVD model at the observed points (b) P1 and (c) P2.

https://doi.org/10.5194/nhess-2024-131
Preprint. Discussion started: 18 September 2024


Natural Hazards and Earth System Sciences Discussions

5.1 Case delineation

Regarding Case A, the "100% bed slopes" scenario in the extended efficiency evaluation section of Chang et al. (2022) is utilized. The used DEM with a 2.5 m grid resolution under the normal grid system is the real-scale Toce River Valley terrain with buildings in a staggered layout (Testa et al., 2007). The Manning roughness coefficient is given as 0.025 $s/m^{1/3}$ according to Chang et al. (2024). For constructing the fine grid system, the original DEM is interpolated into a grid resolution of 1.25 m by the inverse density weight (IDW) interpolation method, leading to 219,856 cells. The short-duration heavy rainfall event is replaced with a fluvial flood event. The high inflow hydrograph by Testa et al. (2007) is scaled back to the original scale and prescribed on the left edge of the computational domain. The simulation duration is given as 6 hours to let the flows gradually recede.

Cases B and C use the layout and settings in Sect. 4.4, including the terrain, land use, sewer network, and "*pollutant releases*" regions, to prepare pollutant events in the pluvial and fluvial flood events. The pluvial flood of Case B is driven by assigning the collected rainfall data on the Ziguan rain gauge (location displayed in Fig. 6b of Wang et al. (2024)) of a historical 23 August 2018 event (rainfall series drawn in Fig. 6e of Wang et al. (2024)) onto the terrain. The released water flows across the whole terrain and causes flooding in the low-lying areas of the terrain, as shown in Fig. 7a of Wang et al. (2024). Case C introduces a fluvial flood by assigning a historical overbank hydrograph in 2016 Typhoon Megi (see Fig. 6f of Wang et al. (2024)) at a breach point in the upstream edge of the terrain (location is drawn in Fig. 6b of Wang et al. (2024)). The released water flows along the low-lying valley in the eastern part of the terrain so that the caused flooding has greater water depths and higher water velocities because of the terrain, as reported in Fig. 7c of Wang et al. (2024). On the other hand, concerning the normal and fine grid systems, the 20 m-resolution DEM with 28,743 cells is regarded to be under the normal grid system. The fine grid system with a grid resolution of 10 m is created by the IDW interpolation method, resulting in a DEM with 114,972 cells. The simulation duration is 24 hours.

As to the settings for solute simulations, for Case A, a time-invariant solute concentration with a value of 1 kg/m^3 is prescribed on the left edge of the simulated terrain where the dambreak flows are released. The other edges are set as outlet boundary conditions to let the released solutes freely leave. Cases B and C use the same solute settings as Wang et al. (2024), *i.e.*, pollutants are released in an initial concentration of 1000 ppm, and a material decay of k=0.02 1/hr and N=1. The diffusion coefficients are computed by the approach of Liang et al. (2010), see Eqs. 17-18 of Wang et al. (2024).

5.2 Efficiency assessment

The run times of the FV-based, CA-based, and GPU-parallelized CA-based approaches are recorded to conduct the assessment. Additionally, the present study also records the run times of the FV-HLLC model, SWFCA, GPU-parallelized SWFCA solver, FV-TVD model, ASTCA solver, and GPU-parallelized ASTCA solver to make a detailed analysis. It is noted that these run times exclude the run times for assigning the boundary conditions and determining the new adaptive time step. The aforementioned run times in the six scenarios are recorded and displayed in Table 2.

https://doi.org/10.5194/nhess-2024-131
Preprint. Discussion started: 18 September 2024

Natural Hazards and Earth System Sciences Discussions

Table 2: The efficiency analysis of the CA-based couple approach through three real-world cases with six scenarios.

Case	Grid resolution	The FV-based coupled approach		The CA-based coupled approach			The GPU-parallelized CA-based coupled approach		
		The FV-HLLC model	The FV-TVD model	The SWFCA solver	The ASTCA solver	Total run time	The GPU-parallelized SWFCA solver	The GPU-parallelized ASTCA solver	Total run time
	(m)	Run time (s)	Run time (s)	Run time (s)	Run time (s)	Run time (s)	Run time (s)	Run time (s)	Run time (s)
		(1)	(2)	(3)	(4)	(5)=(3)+(4)	(6)	(7)	(8)=(6)+(7)
A	2.5	450.9	469.7	351.6	155.3	506.9	6.1	2.9	9.0
	1.25	4787.8	5148.2	3678.8	1601.6	5280.4	57.3	26.4	83.7
B	20	248.8	253.1	192.9	87.4	280.3	2.9	1.4	4.3
	10	1204.5	1254.6	919.6	416.1	1335.7	13.1	5.9	19.0
C	20	239.5	247.7	188.6	74.4	263.0	2.6	1.1	3.7
	10	1338.3	1423.7	1006.2	447.2	1453.4	13.2	6.4	19.6
Average ratio (%)		48.9%	51.1%	69.6%	30.4%	100.0%	68.4%	31.6%	100.0%

Efficiency

				The speed-up ratio (9)=(1)/(3)	The speed-up ratio (10)=(2)/(4)		The speed-up ratio (11)=(3)/(6)	The speed-up ratio (12)=(4)/(7)	The speed-up ratio (13)=(5)/(8)
A	2.5			1.28	3.02		57.64	53.55	56.32
	1.25			1.30	3.21		64.20	60.67	63.09
B	20			1.29	2.90		66.62	62.43	65.19
	10			1.31	3.02		70.20	70.53	70.30
C	20			1.27	3.33		72.54	67.64	71.08
	10			1.33	3.18		76.23	69.88	74.15

Based on the computed speed-up ratios in Table 2, the SWFCA solver is found to be faster than the FV-HLLC model by 1.28-1.30 times, which complies with the outcome of Chang et al. (2022). As to the ASTCA solver, its efficiency is increased up to 2.90-3.33 times compared to the FV-TVD model, which is close to the STMCA solver in Chang et al. (2022) but with higher accuracy found in this research. Thus, the STMCA solver is both more accurate and efficient than the state-of-the-art FV-TVD model. On the other hand, after implementing the GPU parallelization, the SWFCA solver, ASTCA solver, and the CA-based approach enlarge their efficiency up to 57.64-66.62, 53.55-62.43, and 56.32-74.15 times, respectively. This outcome is quite satisfactory since the simulations are performed on a simple PC equipped with a graphic card that is not subjected to high-performance parallel computing. The speed-up ratios are expected to be higher if more advanced equipment can be used. Consequently, the GPU-parallelized SWFCA solver, ASTCA solver, and proposed approach are all demonstrated to be efficient tools in real-world simulations. Nevertheless, the speed-up ratios of the GPU-parallelized SWFCA solver are relatively larger than those of the GPU-parallelized ASTCA solver, which is because the

https://doi.org/10.5194/nhess-2024-131
Preprint. Discussion started: 18 September 2024


Natural Hazards and Earth System Sciences Discussions

SWFCA solver has more steps to be GPU-parallelized than the ASTCA solver. Nevertheless, inspection of the average ratios in Table 2 reveals that the original and GPU-parallelized SWFCA solvers consume most of the run times (68.4%-69.6%). Thus, the SWFCA solver still remains to be the bottleneck. Interestingly, for the FV-based approach, the FV-TVD model consumes more run times than the FV-HLLC model because it requires more operations for extrapolations and gradient computations.

6 Conclusions

The present study establishes a coupled approach that comprises the SWFCA solver for dynamic-wave flow modeling and a new ASTCA solver for solute transport modeling. Additional treatments have been developed into the ASTCA solver to further increase the accuracy in flows with high Péclet numbers. The CA-based coupled approach is then GPU-parallelized by using OpenCL 2.1 under Nvidia CUDA. The accuracy of the newly developed ASTCA solver is first verified and compared to a FV-TVD model through four test cases. Next, the efficiency of the original and GPU-parallelized CA-based coupled approaches is assessed through three real-world cases with massive computational cells. An efficiency comparison is also performed by using a FV-based coupled approach that consists of a popularly used FV-HLLC model for flood flows and the FV-TVD model for solute transport. All of the simulations are conducted on an Intel (R) Core (TM) i9 PC with 6.0 GB RAM and an Intel (R) UHD Graphics 630 graphic card. Based on the simulated results, the conclusions are drawn as follows.

Concerning numerical accuracy, the ASTCA solver has much better accuracy than the STMCA solver and FV-TVD model, particularly in the advection-dominated scenarios with rectangle-shaped/triangle-shaped/trapezoidal-shaped profiles. As for numerical efficiency, compared to the FV-HLLC and FV-TVD models, the SWFCA and ASTCA solvers are found to increase the efficiency up to 1.28-1.33 and 2.90-3.33 times, respectively. Thus, the ASTCA solver is more accurate and efficient than the state-of-the-art FV-TVD model. After implementing GPU parallelization, the SWFCA solver, ASTCA solver, and CA-based approach achieve accelerations of 57.64-76.23, 53.55-69.88, and 56.32-74.15 times, respectively. This outcome is satisfying since the simulations are performed on a PC without a high-level graphic card for parallel computing. Hence, the proposed CA-based approach has been proven to be a useful tool for real-world flood flows and solute transport simulations.

Code availability

Concerning the used numerical models, in shallow water flow modeling, the FV-HLLC model is the “HLLC scheme” described by Yu and Chang (2021). The full description of the SWFCA solver can be found in Chang et al. (2022). As for solute transport modeling, the FV-TVD model's computing methodology in the present research comes from Liang (2010).

https://doi.org/10.5194/nhess-2024-131
Preprint. Discussion started: 18 September 2024


Natural Hazards and Earth System Sciences Discussions

As for the STMCA solver, the readers are referred to Wang et al. (2024) for the complete description of its computing methodology. The ASTCA solver built in this research is extensively introduced in Sect. 2, where the workflow for the CA-based couple approach is given in this section as well. The strategy for GPU implementation on the CA-based coupled approach is given in Sect. 3.

Data availability

The data used for Cases 1-2 in model verification can be reproduced directly by the descriptions given in the texts. The data for Case 3 in model verification is from Morris (2000). The data for Case 4 in model verification, including the digital elevation model (DEM), ground use, locations of the two observed points, polygon for the "pollutant release" regions, and historical rainfall data, can be downloaded from the URL provided by the present study https://www.space.ntu.edu.tw/navigate/a/#/s/D4C6ADB06F934BB4BCCAB47BF68E08476BL. Data for Case A in model efficiency assessment can be prepared by using the data by Testa et al. (2007). Data for Case B in model efficiency assessment can be derived by using data from Case 4 in model verification. Data for Case C in the model efficiency assessment is prepared by using the data of Case B with additional information about the location of the breach point and the assigned historical overbank hydrograph at the breach point, which are also given in the aforementioned URL. Figures in Sects. 2 and 3 are drawn by Microsoft PowerPoint version 2019. Figures in Sect. 4 (model verification) are made with Matplotlib version 3.7.3, available under the Matplotlib license at https://matplotlib.org/.

Author contribution

Hsiang-Lin Yu designed the computing methodology; Hsiang-Lin Yu developed the ASTCA solver and combined it with the SWFCA solver as a coupled approach; Hsiang-Lin Yu and Tsang-Jung Chang analyzed the data and drew the result figures; Hsiang-Lin Yu wrote the manuscript draft; Hsiang-Lin Yu and Tsang-Jung Chang edited the manuscript.

Competing interests

The authors declare that they have no conflict of interest.

https://doi.org/10.5194/nhess-2024-131
Preprint. Discussion started: 18 September 2024


Natural Hazards and Earth System Sciences Discussions

References

Addison-Atkinson, W., Chen, A.S., Memon, F.A. and Chang, T.J.: Modelling urban sewer flooding and quantitative microbial risk assessment: A critical review, J. Flood Risk Manag., 15(4), e12844, 1-29, 2022.

Castro-Orgaz, O. and Hager, W.H.: Shallow Water Hydraulics, Springer, Switzerland, 2019.

Caviedes-Voullième, D., Fernández-Pato, J. and Hinz, C.: Cellular automata and finite volume solvers converge for 2D shallow flow modelling for hydrological modelling, J. Hydrol., 563, 411-417, 2018.

Caviedes-Voullième, D., Fernández-Pato, J. and Hinz, C.: Performance assessment of 2D Zero-Inertia and Shallow Water models for simulating rainfall-runoff processes, J. Hydrol., 584: 124663, 1-20, 2020.

Chang, K.H., Wu, Y.T., Wang, C.H. and Chang, T.J.: A new 2D ESPH bedload sediment transport model for rapidly varied flows over mobile beds, J. Hydrol., 634: 131002, 1-13, 2024.

Chang, T.J., Chang, K.H. and Kao, H.M.: A new approach to model weakly nonhydrostatic shallow water flows in open channels with smoothed particle hydrodynamics, J. Hydrol., 519, 1010-1019, 2014.

Chang, T.J., Chang, Y.S. and Chang, K.H.: Modeling rainfall-runoff processes using smoothed particle hydrodynamics with mass-varied particles, J. Hydrol., 543, 749-758, 2016.

Chang, T.J., Kao, H.M., Chang, K.H. and Hsu, M.H.: Numerical simulation of shallow-water dam break flows in open channels using smoothed particle hydrodynamics, J. Hydrol., 408, 78-90, 2011.

Chang, T.J., Yu, H.L., Wang, C.H. and Chen, A.S.: Overland-gully-sewer (2D-1D-1D) urban inundation modeling based on cellular automata framework, J. Hydrol., 603: 127001, 1-16, 2021.

Chang, T.J., Yu, H.L., Wang, C.H. and Chen, A.S.: Dynamic-wave cellular automata framework for shallow water flow modelling, J. Hydrol., 613: 128449, 1-21, 2022.

Chang, Y.S. and Chang, T.J.: SPH simulations of solute transport in flows with steep velocity and concentration gradients, Water, 9, 132, 1-17, 2017.

Costabile, P., Costanzo, C. and Macchione, F.: Performances and limitations of the diffusive approximation of the 2-d shallow water equations for flood simulation in urban and rural areas, Appl. Numer. Math., 116, 141-156, 2017.

Dazzi, S., Vacondio, R., Palù, A.D. and Mignosa, P.: A local time stepping algorithm for GPU-accelerated 2D shallow water models, Adv. Water Resour., 111, 274-288, 2018.

Dottori, F. and Todini, E.: Developments of a flood inundation model based on the cellular automata approach: testing different methods to improve model performance, Phys. Chem. Earth Parts ABC, 36, 266-280, 2011.

Ghimire, B., Chen, A.S, Guidolin, M., Keedwell, E.C., Djordjević, S. and Savić, D.A.: Formulation of a fast 2D urban pluvial flood model using a cellular automata approach, J. Hydroinform., 15, 676, 1-11, 2013.

Ginzburg, I., Roux, L. and Silva, G.: Local boundary reflections in lattice Boltzmann schemes: spurious boundary layers and their impact on the velocity, diffusion and dispersion, C. R. Mecanique, 343, 518-532, 2015.

https://doi.org/10.5194/nhess-2024-131
Preprint. Discussion started: 18 September 2024


Natural Hazards and Earth System Sciences Discussions

Gordillo, G., Morales-Hernández, M., Echeverribar, I., Fernández-Pato, J. and García-Navarro, P.: A GPU-based 2D shallow water quality model, J. Hydroinform., 22, 1182, 1-16, 2020.

Guidolin, M., Chen, A.S., Ghimire, B., Keedwell, E.C., Djordjević, S. and Savić, D.A.: A weighted cellular automata 2D inundation model for rapid flood analysis, Environ. Modell. & Softw., 84, 378-394, 2016.

Hou, J., Liang, Q., Li, Z., Wang, S. and Hinkelmann, R.: Numerical error control for second-order explicit TVD scheme with limiters in advection simulation, Comput. Math. Appl., 70, 2197-2209, 2015.

Jahanbazi, M., özgen, I., Aleixo, R. and Hinkelmann, R.: Development of a diffusive wave shallow water model with a novel stability condition and other new features, J. Hydroinform., 19, 405-425, 2017.

Kao, H.M. and Chang, T.J.: Numerical modeling of dambreak-induced flood and inundation using smoothed particle hydrodynamics, J. Hydrol., 448-449, 232-244, 2012.

Lee, M.E. and Seo, I.W.: Analysis of pollutant transport in the Han River with tidal current using a 2D finite element model, J. Hydro-environ. Res., 1, 30-42, 2007.

Liang, D., Wang, X., Falconer, R.A. and Bockelmann-Evans, B.N.: Solving the depth-integrated solute transport equation with a TVD-MacCormack scheme, Environ. Modell. & Softw., 25, 1619-1629, 2010.

Liang, Q.: A well-balanced and non-negative numerical scheme for solving the integrated shallow water and solute transport equations, Commun. Comput. Phys., 7, 1049-1075, 2010.

Lin, L. and Liu, Z.: TVDal: Total variation diminishing scheme with alternating limiters to balance numerical compression and diffusion, Ocean Model., 134, 42-50, 2019.

Liu, W., Hou, Q., Lian, J., Zhang, A. and Dang, J.: Coastal pollutant transport modeling using smoothed particle hydrodynamics with diffusive flux, Adv. Water Resour., 146: 103764, 1-11, 2020.

Martins, R., Leandro, J. and Djordjević, S.: Wetting and drying numerical treatments for the Roe Riemann scheme, J. Hydraul. Res., 56, 256-267, 2018.

Milašinović, M., Ranđelović, A., Jaćimović, N. and Prodanović, D.: Coupled groundwater hydrodynamic and pollution transport modelling using Cellular Automata approach, J. Hydrol., 576, 652-666, 2019.

Morales-Hernández, M., Murillo, J. and García-Navarro, P.: Diffusion-dispersion numerical discretization for solute transport in 2D transient shallow flows, Environ. Fluid Mech., 19, 1217-1234, 2019.

Sanders, B.F. and Schubert, J.E.: PRIMo: Parallel raster inundation model, Adv. Water Resour., 126, 79-95, 2019.

Sarkhosh, P. and Jin, Y.C.: MPS-based model to solve one-dimensional shallow water equations, Water Resour. Res., 57, e2020WR028742, 2021.

Testa, G., Zuccala, D., Alcrudo, F., Mulet, J. and Soares-Frazão S.: Flash flood flow experiment in a simplified urban district, J. Hydraul. Res., 45, 37-44, 2007.

Tian, L., Gu, S., Wu, Y., Wu, H. and Zhang, C.: Numerical investigation of pollutant transport in a realistic terrain with the SPH-SWE method, Front. Environ. Sci., 10: 889526, 1-12, 2022.

Toro, E.F.: Shock-Capturing Methods for Free-Surface Shallow Flows, John Wiley, New York, 2001.

https://doi.org/10.5194/nhess-2024-131
Preprint. Discussion started: 18 September 2024


Natural Hazards and Earth System Sciences
Discussions

Wang, H., Cater, J., Liu, H., Ding, X. and Huang, W.: A lattice Boltzmann model for solute transport in open channel flow, J. Hydrol., 556, 419-426, 2018.

Wang, C.H., Yu, H.L. and Chang, T.J.: A novel cellular automata framework for modeling depth-averaged solute transport during pluvial and fluvial floods, Water, 16 (1), 129, 1-23, 2024.

Yu, H.L. and Chang, T.J.: A hybrid shallow water solver for overland flow modelling in rural and urban areas, J. Hydrol., 598: 126262, 1-17, 2021.

Yu, H.L and Chang, T.J.: GPU parallelization of particulate matter concentration modeling in indoor environment with cellular automata framework, Build. Environ., 243: 110724, 1-10, 2023.

Zhang, L., Liang, Q., Wang, Y. and Yin, J.: A robust coupled model for solute transport driven by severe flow conditions, J. Hydro-environ. Res., 9, 49-60, 2015.

Zhao, J. and Liang, Q.: Novel variable reconstruction and friction term discretization schemes for hydrodynamic modelling of overland flow and surface water flooding, Adv. Water Resour., 163: 104187, 1-19, 2022.